JMR Journal of Meteorological Research

Springer PIIJ

Estimation of Gridded Atmospheric Oxygen Consumption from 1975 to 2018

Xiaoyue LIU, Jianping HUANG, Jiping HUANG, Changyu LI, Lei DING, Wenjun MENG

Citation: Liu, X. Y., J. P. Huang, J. P. Huang, et al., 2020: Estimation of gridded atmospheric oxygen consumption from 1975 to 2018. *J. Meteor. Res.*, **34**(3), 646–658, doi: 10.1007/s13351–020–9133–7

View online: http://jmr.cmsjournal.net/article/doi/10.1007/s13351–020–9133–7

Estimation of Gridded Atmospheric Oxygen Consumption from 1975 to 2018

Xiaoyue LIU[1], Jianping HUANG[1*], Jiping HUANG[2], Changyu LI[1], Lei DING[1], and Wenjun MENG[3]

1 *Collaborative Innovation Center for Western Ecological Safety*, *Lanzhou University*, *Lanzhou* 730000, *China*
2 *Enlightening Bioscience Research Center*, *Mississauga L4X 2X7*, *Canada*
3 *Laboratory for Earth Surface Processes*, *College of Urban and Environmental Sciences*, *Peking University*, *Beijing* 100871, *China*

(Received September 6, 2019; in final form February 2, 2020)

ABSTRACT

Atmospheric Oxygen (O_2) is one of the dominating features that allow the earth to be a habitable planet with advanced civilization and diverse biology. However, since the late 1980s, observational data have indicated a steady decline in O_2 content on the scale of parts-per-million level. The current scientific consensus is that the decline is caused by the fossil-fuel combustion; however, few works have been done to quantitatively evaluate the response of O_2 cycle under the anthropogenic impact, at both the global and regional scales. This paper manages to quantify the land O_2 flux and makes the initial step to quantificationally describe the anthropogenic impacts on the global O_2 budget. Our estimation reveals that the global O_2 consumption has experienced an increase from 33.69 ± 1.11 to 47.63 ± 0.80 Gt (gigaton, 10^9 t) O_2 yr^{-1} between 2000 and 2018, while the land production of O_2 (totaling 11.34 ± 13.48 Gt O_2 yr^{-1} averaged over the same period) increased only slightly. In 2018, the combustion of fossil-fuel and industrial activities (38.45 ± 0.61 Gt O_2 yr^{-1}) contributed the most to consumption, followed by wildfires (4.97 ± 0.48 Gt O_2 yr^{-1}) as well as livestock and human respiration processes (2.48 ± 0.16 and 1.73 ± 0.13 Gt O_2 yr^{-1}, respectively). Burning of fossil-fuel that causes large O_2 fluxes occurs in East Asia, India, North America, and Europe, while wildfires that cause large fluxes in comparable magnitude are mainly distributed in central Africa.

Key words: oxygen (O_2) cycle, climate change, anthropogenic activities

Citation: Liu, X. Y., J. P. Huang, J. P. Huang, et al., 2020: Estimation of gridded atmospheric oxygen consumption from 1975 to 2018. *J. Meteor. Res.*, **34**(3), 646–658, doi: 10.1007/s13351-020-9133-7.

1. Introduction

The global carbon cycle has responded forcefully under the impact of increasingly intensive human activities, which has already been addressed by voluminous literature on both the global and regional scales in the recent decades (Huang et al., 2007; Luyssaert et al., 2007; Li et al., 2012; IPCC, 2014; Chen et al., 2017). Knowledge of this process is not only essential for understanding the history of earth system, but also of critical significance for guiding the future of human beings. In the meantime, as an indispensable component in the global biogeochemical cycle, the oxygen (O_2) cycle is also responding substantially to the global change. The O_2 and carbon cycles are coupled with each other by a variety of processes including respiration and photosynthesis (Keeling and Manning, 2014). However, they also act separately since there are other processes, including the oceanic outgassing of O_2 (mostly due to ocean water warming), photolysis of water, oxidation of minerals, etc., in which carbon doesn't involve (Petsch, 2014; Royer, 2014). Equivalent in magnitude to the increase in atmospheric CO_2, the annual decline in O_2 is approximately an average of 4 ppm yr^{-1}. The dependency of humankind and other living organisms on atmospheric O_2 cannot be overemphasized since an equable O_2 in the atmosphere is pivotal to life (Petsch, 2014). Hence, attention should be paid to the difference between the carbon and O_2 cycles and it is necessary to conduct systematic investigations on the O_2 cycle independently (Shi et al., 2019), especially under the impact of anthropogenic activities. Obviously, burning of fossil-fuel that causes both the increase in CO_2 and decrease in O_2 cannot be diagnosed as the only reason explaining the recent O_2 decline. Other processes,

Supported by the National Natural Science Foundation of China (41521004) and China 111 Project (B13045).

*Corresponding author: hjp@lzu.edu.cn.

including respiration, photosynthesis, burning of organic matters, etc., should also be taken into account (Huang et al., 2018).

Previous studies have assumed that a constant atmospheric O_2 concentration remains under the condition that individual components of the budget are time-independent (Bender et al., 1994a, b). However, ever since the Industrial Revolution, extensive fossil-fuel combustions have emitted a substantial volume of CO_2 into the atmosphere (IPCC, 2014; Zhai et al., 2018), and simultaneously removed substantial amounts of O_2. This has resulted in changes in both the CO_2 and O_2 cycles on the same order of magnitude as the natural variability. The polar ice core analysis indicates that the decline in atmospheric O_2 is related to burning of fossil-fuel since the beginning of the Industrial Revolution (Battle et al., 1996). Previous research has shown that cumulative emissions from the fossil-fuel and land-use change were 615 ± 80 Gt C, which were portioned among the atmosphere (25 ± 5 Gt C), ocean (150 ± 20 Gt C), and land (190 ± 50 Gt C; Le Quéré et al., 2018). However, it seems that discussions on the individual feedback of each member in the O_2 cycle to human activities are currently lacking. Quantitative estimations of each component and its temporal variation (e.g., O_2 production from terrestrial and oceanic ecosystems, O_2 consumption due to human activities, etc.) in the O_2 cycle are needed to reveal the response of O_2 cycle under the background of human-induced climate changes.

In addition, past studies considered the O_2 budget only at the global scale and roughly presented the global average value of each component. Nevertheless, the consumption and production of O_2 over land are not uniform and may vary with locations due to the intensity of human activities (e.g., economic development, population density, etc.) and natural conditions (vegetation coverage, phenology, etc.). In some areas where massive anthropogenic O_2 fluxes occur, the local O_2 consumption can far exceed its local production; maintaining local O_2 levels then requires O_2 transport from other regions where production exceeds the consumption via atmospheric circulation. Therefore, a global O_2 budget on a grid scale needs to be established to map the spatial characteristics of O_2 budget, which helps to identify the source and sink of atmospheric O_2 in the warming climate. The result is promised to provide a novel viewpoint in assessing the ecological security, sustainable development, habitability for human settlements, etc., from the perspective of atmospheric O_2.

In this paper, we present a systematic estimation of global O_2 consumption on a resolution of 1.0° × 1.0° over the globe. The product covers four major types of O_2 consumption processes (fossil-fuel combustion, respiration of human and livestock, and wildfires). We also compare our data with the O_2 production from the terrestrial ecosystem and present an O_2 balance over land. At the end of this paper, data uncertainties are estimated by using the Monte Carlo method, and we validate our estimated O_2 fluxes against observations. The O_2 flux data proposed in this paper can be downloaded at https://doi.org/10.1594/PANGAEA.899167 with a resolution of 1.0° × 1.0° ranging from 1975 to 2018 (Liu et al., 2019).

2. Datasets and methods

2.1 *Estimation of global O_2 fluxes*

In this study, the four O_2 consumption processes listed in Table 1 are considered. The contribution from long timescale processes, such as oxidation and weathering, are negligible compared with the short O_2 cycle timescale considered here (Royer, 2014; Stolper et al., 2016). With regards to the wildfire-induced O_2 flux, some of the wildfires are natural ones, while others are started by humans, e.g., burning of agricultural waste and deforestation. In the quantification of O_2 balance in the terrestrial ecosystem, the wildfire component is included as part of O_2 consumption fluxes and it is excluded from O_2 production fluxes from terrestrial ecosystems (see Section 3.4). An overview of the data sources used to estimate global O_2 fluxes is shown in Table 1.

2.1.1 *O_2 fluxes due to consumption by fossil-fuel combustion*

The comprehensive information from the Carbon Dioxide Information Analysis Center (CDIAC; Andres et al., 2016), the Open-source Data Inventory for Anthropogenic CO_2 (ODIAC; http://www.odiac.org/), the Emissions Database for Global Atmospheric Research (EDGAR; Janssens-Maenhout et al., 2019), and the PKU (Peking University)-CO_2 (Wang et al., 2013; Liu et al., 2015; http://inventory.pku.edu.cn/) are collected. The EDGAR data estimate the emissions according to the emission sectors specified by the Intergovernmental Panel on Climate Change (IPCC) methodology and distinguish between (1) long-cycle CO_2 emission from fossil-fuel and industrial processes (the "CO2_excl_short-cycle_org_C" data) and (2) short-cycle CO_2 emission, including agriculture burning (the "CO2_short-cycle_org_C"), etc. In this paper, the "CO2_excl_short-cycle_org_C" data of EDGAR are selected since the short-cycle burning processes are considered in other components of our estimation (wildfires). As for CDIAC,

Table 1. Data sources used in this study to estimate the global O_2 flux

Component	Sub-component	Data source	Time	Spatial resolution
Fossil-fuel combustion	Solid fuel (coal)	CDIAC[1]	1751–2013	1° × 1°
	Liquid fuel (oil)	EDGARv5.0	1970–2018	0.1° × 0.1°
	Gas fuel (natural gas)	ODIAC2018	2000–2017	1° × 1°
	Flared gas Biofuel	PKU-CO_2	1960–2014	0.1° × 0.1°
Human respiration	Male and female	World Population Prospects 2019	1950–2020	National data
		Global dataset of gridded population and GDP scenarios	1980–2100	0.5° × 0.5°
Livestock respiration	Buffaloes, cattle, chicken, ducks, goats, horses, pigs, and sheep	Gridded livestock data	2010	5′ × 5′
Wildfire	Agricultural waste burning, boreal forest fires, peat land fires, temperate forest fires, tropical forest fires, and savanna fires	Global fire emissions database, version 4.1 (GFED v4)	1997–2016	0.25° × 0.25°

[1] Both the gridded annual emission estimates and national tabular data from CDIAC were used.

ODIAC-2018, and PKU-CO_2, the data that only cover the emissions from fossil-fuel burning are used in this paper. Therefore, the global total CO_2 emission in EDGAR is slightly higher (about 1.5 Gt CO_2 a^{-1}) than that in the other three datasets, because EDGAR includes the emissions from industrial processes (chemical production, metal production, etc.).

Carbon emissions from the above-mentioned data sources are aggregated and the ensemble mean of carbon emissions is calculated for the conversion from carbon to O_2 fluxes. The O_2 flux due to consumption by fossil-fuel combustion can be converted from the emission of carbon according to the chemical equation below:

$$\mathrm{C}_x\mathrm{H}_y + \left(x + \frac{1}{4}y\right)\mathrm{O}_2 \rightarrow x\mathrm{CO}_2 + \frac{1}{2}y\mathrm{H}_2\mathrm{O}. \quad (1)$$

Due to fuel differences among countries, the oxidative ratio [OR—the number of O_2 moles consumed per mole of CO_2 emitted, $\left(x + \frac{1}{4}y\right)$] can exhibit spatial and temporal variations (Steinbach et al., 2011). In this study, the carbon emitted by each type of fossil fuels in each grid is derived from the PKU-CO_2 data and used to calculate OR_i (where index i indicates the fuel type) for each grid. We use the ensemble mean of CDIAC, ODIAC, EDGAR, and PKU-CO_2 for carbon emission data (E_{FF}). Based on the equation below, the O_2 flux by fossil fuel can thus be estimated:

$$C_{\mathrm{FF}} = E_{\mathrm{FF}} \times \mathrm{OR} \times \frac{M_{\mathrm{O}_2}}{M_{\mathrm{C}}}, \quad (2)$$

where C_{FF} is the annual O_2 flux (Gt O_2 yr^{-1}) per grid; E_{FF} is the carbon emissions from fossil-fuel combustion (Gt C yr^{-1}) per grid; M_{O_2} is the relative molecular mass of O_2 (32 g mol^{-1}); M_{C} is the relative molecular mass of carbon (12 g mol^{-1}); and OR is the molar ratio O_2/CO_2 per grid at the time of burning. OR is calculated based on the following equation:

$$\mathrm{OR} = \frac{\sum_{i=1}^{4} E_{\mathrm{FF}_i} \times \mathrm{OR}_i}{E_{\mathrm{FF}}}, \quad (3)$$

where again, i indicates the fuel type.

The OR of each fuel type is presented in Table 2, with a 90% confidence interval. We consider four fuel types: solid fuel (coal), liquid fuel (oil), gas fuel (natural gas), and biomass. The ORs for solid, liquid, and gas fuels are calculated after Keeling (1988), and that for biomass is based on Steinbach et al. (2011), with an assumed confidence interval of 0.03. In the PKU-CO_2 data, emissions from the flared gas are integrated into gas fuel ones. These two types of emissions have similar ORs (1.98 for flared gas and 1.95 for gas, respectively). For simplicity, we make the assumption that their ORs are equal.

2.1.2 *O_2 fluxes due to human respiration*

The estimation of O_2 fluxes due to human respiration is derived from the population density and daily total energy expenditure (TEE). Population densities of males and females are spatially distributed in the following way. The coarse-scale country totals of males and females from the 2019 Revision of World Population Prospects (United Nations et al., 2019) are mapped onto a 1.0° × 1.0° grid by using the spatial distribution of population density from Murakami and Yamagata (2019).

Jones (2003) estimated that for survival the daily O_2 consumption for an astronaut is about 0.84 kg O_2 day^{-1}.

Table 2. The oxidative ratio (OR) for each fuel type

Fuel type	O_2/CO_2 molar ratio
Solid fuel (coal)	1.17 ± 0.03
Liquid fuel (oil)	1.44 ± 0.03
Gas fuel (natural gas)	1.95 ± 0.04
Flared gas	1.98 ± 0.07
Biofuel	1.07 ± 0.03

We estimate the daily O_2 consumption based on daily TEE (Walpole et al., 2012), defined as the product of basal metabolic rate (BMR) and physical activity level (PAL). BMR is determined by a variety of factors, including the sex, age, and weight. The BMRs at different ages are listed in Table 3 (Henry, 2005). The percentage of population at different age groups is calculated based on the 2019 Revision of World Population Prospects (United Nations et al., 2019). The weighted averages of BMRs in different age groups for males and females are calculated to obtain TEEs of males and females with moderate activity levels (PAL of 1.76 ± 0.1 for males and 1.64 ± 0.1 for females), and the TEES are 9.69 and 7.85 MJ day^{-1}, respectively. To convert TEE to O_2 consumption, the average value of O_2 thermal equivalent (20.2 kJ L^{-1} O_2, usually varies by the individual diet) is used (Dintenfass et al., 1983; Frape, 2008). On this basis, O_2 consumption values of men and women are 0.69 and 0.55 kg day^{-1}, lower than that estimated for an astronaut. This is because the elderly and children, who consume less O_2 than young adults, are taken into account. We estimate the total O_2 consumption due to human respiration with the formula below:

$$C_{\mathrm{RES}-H} = \frac{(P \times \mathrm{BMR} \times \mathrm{PAL})_{\mathrm{male}} + (P \times \mathrm{BMR} \times \mathrm{PAL})_{\mathrm{female}}}{\mathrm{TEO}} \times \rho_{\mathrm{O_2}} \times 365, \quad (4)$$

where $C_{\mathrm{RES}-H}$ denotes the O_2 consumed by human breathing annually (Gt O_2 yr^{-1}); P_{male} and P_{female} are the total male and female populations of each grid, respectively; TEO is the thermal equivalent of O_2; and $\rho_{\mathrm{O_2}}$ is the atmospheric O_2 density (1.429 g L^{-1} at standard atmospheric temperature and pressure).

2.1.3 *O_2 fluxes due to livestock respiration*

On the basis of the gridded data of livestock population with a resolution of 0.083° [Gridded Livestock of the World (GLW 3); Gilbert et al., 2018], in which the global population densities of eight types of livestock (buffaloes, cattle, chickens, ducks, goats, horses, pigs, and sheep) are provided, O_2 consumption due to livestock respiration is estimated. In the areal-weighted version of this data set, animal numbers are evenly distributed in areas where the censuses are conducted for each type of livestock.

The mammal BMR can be estimated by the equation BMR = $3.43M^{0.75}$ (Kleiber, 1932), in which M is the mass of the mammal (g). Thus, calculations of the annual O_2 consumption by livestock can be done according to the formula below:

$$C_{\mathrm{RES}-L} = \sum_{i=1}^{6} P_i \times \mathrm{BMR}_{\mathrm{d}i} \times \mathrm{PAL} \times \mathrm{LS}_i, \quad (5)$$

where $C_{\mathrm{RES}-L}$ represents the O_2 consumed by livestock annually (Gt O_2 yr^{-1}); P_i denotes the total number of livestock of type i; $\mathrm{BMR}_{\mathrm{d}i}$ refers to the average daily O_2 consumption by livestock of type i (kg O_2 day^{-1}); PAL is the physical activity level (1.2 ± 0.1); and LS_i is the lifespan of livestock of type i (see Table 4).

The data derived from GLW 3 are in 2010. When the population increases, the livestock and agriculture industry should be developed to meet the growing food demand. In addition, we compared the time series of population and global total number of cattle (data from http://www.fao.org/faostat/en/#home) and found that the variation pattern of population is basically consistent with that of cattle. Therefore, when O_2 consumptions for other years are calculated, it is assumed that the number of livestock increase (decrease) with the increase (decrease) in human population at the same scale, and the geographical distribution of original data of livestock is maintained.

2.1.4 *O_2 fluxes due to wildfires*

By converting from the carbon emission data in the GFED v4 (van der Werf et al., 2017) from 1997 to 2018 with a spatial resolution of 0.25°, the O_2 consumption due to wildfires is obtained. Wildfire types are classified into six ones (see Table 1). According to the equation below, wildfire O_2 consumption can be obtained:

$$C_{\mathrm{FIRE}} = M_{\mathrm{O_2}} \times \sum_{i=1}^{6} \frac{\mathrm{DM} \times \mathrm{contr}_i \times \mathrm{EF}_i}{M_{\mathrm{CO_2}}} \times \alpha_B, \quad (6)$$

where C_{FIRE} is the wildfire O_2 consumption (Gt O_2 yr^{-1}); subscript i is used to indicate the fire type; DM is the mass of dry matters emitted (kg DM m^{-2} yr^{-1}); contr_i is

Table 3. BMRs at different age groups

Age	Percentage of population (%)	Weight (kg)		BMR (MJ day^{-1})	
		Male	Female	Male	Female
0–3	6.5	6.30 ± 3.20	6.70 ± 3.40	1.47 ± 0.86	1.54 ± 0.87
3–10	16.4	21.40 ± 5.14	23.60 ± 6.14	4.17 ± 0.58	4.10 ± 0.63
10–18	17.3	40.00 ± 12.48	43.40 ± 12.91	5.51 ± 1.11	5.20 ± 0.80
18–30	14.4	61.00 ± 11.40	53.20 ± 10.04	6.36 ± 1.00	5.24 ± 0.79
30–60	32.3	65.30 ± 12.98	59.10 ± 13.65	6.35 ± 1.03	5.31 ± 0.80
60+	13.2	71.30 ± 14.94	60.00 ± 14.52	6.17 ± 1.09	4.93 ± 0.78

Table 4. The O_2 consumption by livestock respiration

Livestock	Body weight (kg)	Individual respiratory O_2 consumption (kg O_2 yr^{-1})	Annual respiratory O_2 consumption in 2018 (kg O_2 yr^{-1})
Buffaloes	272 ± 30	613.68 ± 71.33	$1.31 \pm 0.14 \times 10^{11}$
Cattle	272 ± 30	613.68 ± 71.33	$1.00 \pm 0.11 \times 10^{12}$
Chicken[1]	0.862 ± 0.1	1.01 ± 0.17	$2.34 \pm 0.06 \times 10^{10}$
Ducks[1]	0.862 ± 0.1	1.01 ± 0.17	$1.90 \pm 0.29 \times 10^{09}$
Goats	36 ± 3	134.66 ± 13.95	$1.46 \pm 0.14 \times 10^{11}$
Horses	260 ± 30	593.26 ± 49.81	$4.15 \pm 0.32 \times 10^{10}$
Pigs[2]	75 ± 10	115.16 ± 16.42	$1.29 \pm 0.13 \times 10^{11}$
Sheep	30 ± 3	117.45 ± 13.04	$1.49 \pm 0.19 \times 10^{11}$
Total			$2.48 \pm 0.16 \times 10^{12}$

[1] We assume that the life span of poultry (chickens and ducks) is 45 ± 5 days.
[2] We assume that the life span of a pig is 180 ± 10 days.

the contribution of dry matter emitted for fire of type i (dimensionless); EF_i is the emission factor of CO_2 (kg g^{-1}) of each fire of type i; and α_B is the molar ratio of O_2/CO_2 (1.1 ± 0.1).

The net effect of wildfires on the carbon/O_2 cycle is debated since burning of biomass is believed to be carbon neutral. However, biomass burning can also be carbon negative or carbon sources, depending on both the amount of CO_2 removed from or released into the atmosphere during its growth and the amount of CO_2 released when it is burned (Tilman et al., 2006). Therefore, it is still necessary to consider the wildfire components when investigating the O_2 cycle.

2.1.5 *O_2 fluxes due to other human-related processes*

Apart from the above-mentioned processes that may consume atmospheric O_2, non-fossil-fuel anthropogenic processes including chemical [ammonia (NH_3) production, nitric acid production, etc.] and metal industries (iron and steel production, etc.) can also consume O_2. However, almost all the non-fossil-fuel processes have been covered in the EDGAR inventory, which is averaged with other data sources of CO_2 emissions. Therefore, our estimation contained the non-fossil-fuel processes that may also consume atmospheric O_2. The global total CO_2 emissions in EDGAR is only about 1.5 Gt yr^{-1} higher than the rest of the three datasets, which proves that the contribution from non-fossil-fuel processes is very small. Furthermore, following IPCC (2006), in which the stoichiometry ratios of related chemical reactions are provided, ORs of these processes are significantly lower than those listed in Table 2. Take the NH_3 production for example: the production of every 1 mol of NH_3 emits 0.44 mol CO_2 and consumes 0.26 mol O_2, with an OR of 0.59. For the metal production, the emission of CO_2 comes from the oxidation of coke, which is one type of fossil fuels listed in Table 2. Therefore, the consumption of O_2 in non-fossil-fuel processes has been covered in this paper. Considering that EDGAR is the only data set that includes these processes, we tripled the weight of EDGAR data when calculating the average (3 for EDGAR and 1 for the other three data sources).

The oxidation of atmospheric pollutants (e.g., photochemical pollutants, etc.) is also believed to influence the O_2 in the atmosphere. However, concentrations of the major atmospheric pollutants are at part-per-billion (ppb) or part-per-trillion (ppm) levels. The complete oxidation of these chemicals is only able to cause an O_2 disturbance at their corresponding magnitudes and may not influence the O_2 variation at the ppm level. Despite of the existence of oxidation processes in the atmosphere, changes in the O_2 concentration due to these processes (at ppb or ppt levels) may not be detected on large spatial scales due to the large background value of O_2. Take one of the major pollutants, N_2O, for example: the total emission of N_2O due to human activities (including the fossil-fuel combustion and chemical industries) to the atmosphere in 2012 was 9.15×10^{-3} Gt (Janssens-Maenhout et al., 2019). Even if we assume that all the elementary O_2 in N_2O comes from the atmosphere, only 3.3×10^{-3} Gt O_2 is consumed annually. If all the N_2O emitted by humans is oxidized in the atmosphere, only about 10^{-3} Gt O_2 will be removed. Therefore, the oxidation of chemical pollutants in the atmosphere is not considered in this paper.

2.2 *Uncertainties in O_2 fluxes based on Monte Carlo simulations*

We estimate uncertainties in our O_2 flux calculations by using an Monte Carlo ensemble simulation. For each grid, 1000 pseudo-random samples of input data are generated according to the probability density function (PDF) specified for each input. For the fossil-fuel consumption, uncertainties lie in E_{FF} and OR. We assume that E_{FF} has a normal distribution with a standard deviation based on discrepancies between the datasets, and

that OR also has a normal distribution with a 90% confidence interval (see Table 2).

For human respiration, the main uncertainty lies in the estimation of daily O_2 consumption, specifically, BMR and TEO. The standard deviation of BMRs for males and females in different age groups are presented in Table 3. In addition, we added a standard deviation of 2% in the percentage of population at each age group. For TEO, the standard deviation is set at 0.2 kJ L^{-1} O_2.

The uncertainty in livestock respiration comes from the estimation of gridded population (P), BMR, PAL, and LS. Population data are based on census data, and the gridded population totals equal the total number of animals registered in the Food and Agriculture Organization of the United Nations (FAO) database (Gilbert et al., 2018). It is difficult to quantify the total population uncertainty, therefore we consider only the uncertainties in BMR, PAL, and LS, as listed in Table 4.

The uncertainty in wildfire calculations lies in the estimated DM, contr_i, EF_i, and α_B. van der Werf et al. (2017) pointed out that due to the difficulty in assessing uncertainties in the various fuel layers, they refrained from estimating the formal uncertainties. If present, these uncertainties may far exceed those in GFED v3 (the previous version of the dataset used here). Therefore, we consider only the uncertainties in EF_i (provided on the GFED website) and α_B (1.1 ± 0.1).

Furthermore, uncertainties due to different time ranges among the datasets, and inconsistency within the datasets may also exist. For example, the CDIAC data are only updated to 2013 while the EDGAR data are updated to 2018. The GFED data have failed to maintain the uncertainty of datasets since 2017 because the burned area data have been upgraded by using a different method. Thus, in order to update our results to the latest year, two versions of our data (the official and beta versions) are prepared. The official version is updated to 2013, with all of the data sources listed in Table 1. The beta version is updated to 2017, in which the data of PKU-CO_2 and CDIAC are not included. The beta version may have not maintained the consistency since 2013 due to the lack of data sources. In the following sections, the beta version of our data is analyzed.

3. Results

3.1 *Estimation of O_2 fluxes due to fossil-fuel combustion*

It has been generally accepted that the fossil-fuel combustion has made the largest contribution to the atmospheric O_2 decline in the past decades (Valentino et al., 2008; Keeling and Manning, 2014; Martin et al., 2017). Figures 1a and b show the distribution of O_2 fluxes due to the fossil-fuel combustion and corresponding OR respectively for 2018. In Fig.1a, the distribution of O_2 consumption is similar to that of the CO_2 emission. The US, Europe, India, and East Asia are identified as the high O_2 consumption regions (with O_2 fluxes greater than 500 g O_2 m^{-2} yr^{-1}), while Africa, Australia, and South America are identified as the low areas. As for the distribution of OR (Fig. 1b), the areas that display small ORs, indicating coal as a primary energy source, are located in South Africa, India, and East Asia, while large ORs (larger than 1.45), implying that the natural gas is regarded as the primary energy source, are located in Russia, central Asia, Canada, and most areas of South America. The highest O_2 fluxes appear over China, the US, India, and Russia. The spatial distribution of OR is basically consistent with that in Steinbach et al. (2011).

The global trend in O_2 consumption is presented in Fig. 2a, where areas covered by warm and cold colors denote the increased and decreased consumptions respectively. The consumption is increasing mainly in Asia, whereas in Europe it shows a downward trend. Figure 2b displays the trend in OR of each grid. Areas including Argentina, Russia, and Europe show an increas-

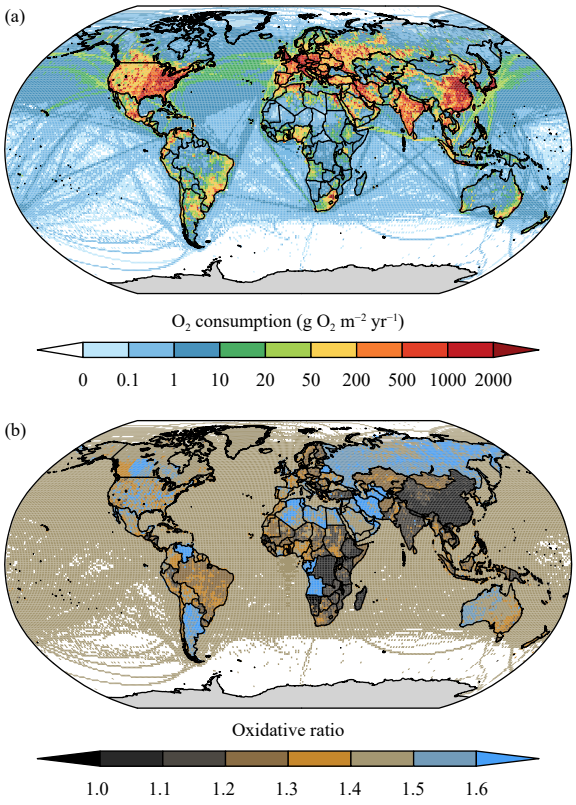

Fig. 1. Global distributions of (a) O_2 fluxes due to fossil-fuel combustion and (b) oxidative ratios (ORs) in 2018.

ing trend while regions such as East Asia and North America show a downward trend. The global total O_2 consumption by fossil fuel increased from 16.6 ± 1.0 to 38.7 ± 0.43 Gt between 1975 and 2018 (Fig. 3).

3.2 *Estimation of O_2 fluxes due to human and livestock respiration*

In the calculation of O_2 fluxes due to human breathing, a moderate PAL of 1.76 is assumed for both males and females. For livestock, we consider eight different types: buffaloes, cattle, chickens, ducks, goats, horses, pigs, and sheep, with a PAL of 1.2. The BMR change due to internal (exercise and diets) and external factors (ambient temperature variation) are not considered (Cai et al., 2018). In this case, true O_2 fluxes due to livestock and humans are likely to be higher than what we estimate here. The global distribution and long-term trends in O_2 fluxes due to human breathing are presented in Fig. 4. The largest O_2 flux (up to 200 g O_2 m^{-2} yr^{-1}) can be found in India and North China, where the largest population density is located. During the past 30 years, the global population has witnessed significant growth, especially in Asia, resulting in an increase in the O_2 consumption there.

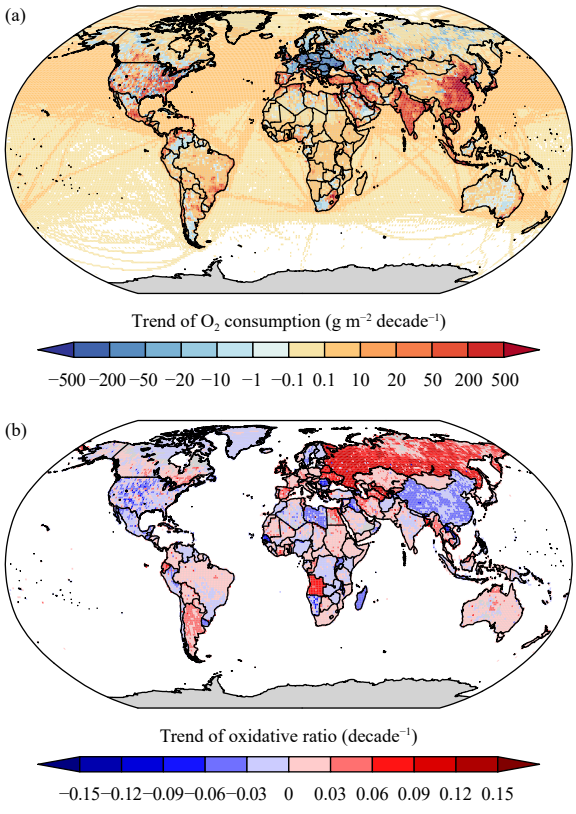

Fig. 2. Global patterns of long-term trend in (a) O_2 fluxes due to the fossil-fuel combustion and (b) ORs during the period of 1975–2018.

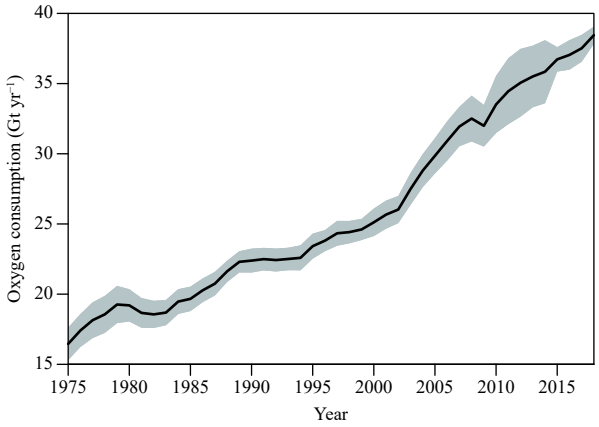

Fig. 3. The trend in total O_2 consumption by fossil-fuel combustion (Gt yr^{-1}) from 1975 to 2018. The standard deviation is denoted by grey shading.

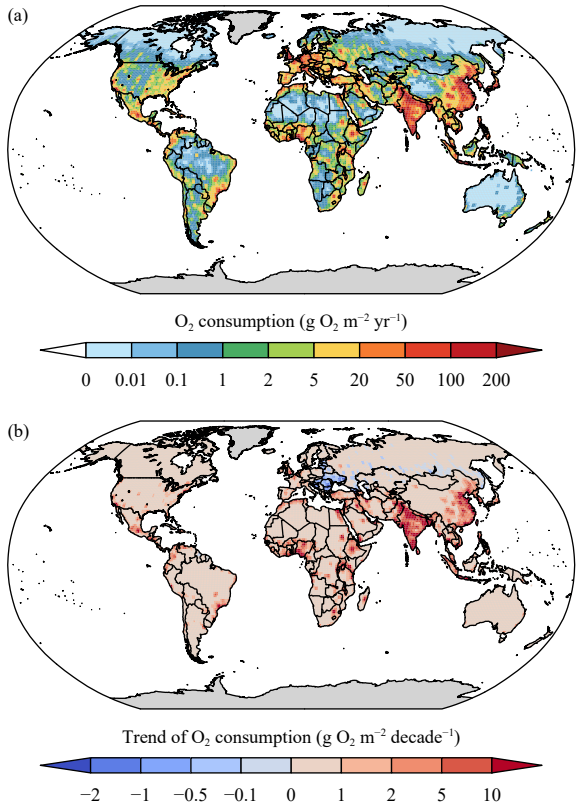

Fig. 4. Global patterns of O_2 fluxes due to human respiration and its long-term trend. (a) O_2 fluxes for 2018 and (b) long-term trends from 1975 to 2018.

The global distribution of O_2 consumption by livestock (Fig. 5) has a basically identical spatial distribution to that of human respiration. This is because the livestock industry is likely to be well-developed to satisfy food demands of a high population density. Human males consumed more O_2 than females in 2018 (0.96 ± 0.10 > 0.76 ± 0.08 Gt O_2 yr^{-1}). When considering the

global total volume, the O_2 consumption due to livestock (2.48 ± 0.16 Gt O_2 yr^{-1}) is slightly larger than that due to human respiration (1.73 ± 0.13 Gt O_2 yr^{-1}) in 2018 (see Fig. 6 and Table 4). Among the eight types of livestock considered in this study, cattle and buffaloes consumed the highest volume of O_2, about 46% of the total O_2 consumption by livestock.

3.3 *Estimation of O_2 fluxes due to wildfires*

The spatial pattern of O_2 fluxes due to wildfires in 2018 is shown in Fig. 7. The highest consumption occurs mainly in the tropics, especially central Africa. This is because abundant surface vegetation exists in these areas, leading to a high value of net primary productivity (NPP). In other words, when wildfires occur in these areas, a higher volume of carbon is released into the atmosphere, which also causes larger O_2 fluxes in the meantime. The global mean O_2 consumption by wildfires is 5.87 Gt O_2 yr^{-1} and displays a weak decline in the period 1997–2018, with a maximum of 7.97 ± 0.8 Gt O_2 yr^{-1} in 1997 and a minimum of 4.82 ± 0.5 Gt O_2 yr^{-1} in 2013. Of the various wildfire types (Fig. 8), savanna fires cover the largest areas around the world and cause the highest O_2 flux, contributing more than 60%; the next-largest O_2 flux is contributed by wildfires in the tropical forests.

3.4 *O_2 balance of the terrestrial ecosystem*

Figure 9 shows the global distribution of averaged net terrestrial O_2 flux from 2000 and 2018. The distribution of O_2 flux (Fig. 9a) has a basically identical pattern to that of O_2 flux due to the fossil fuel. The reason is quite obvious. Among the four O_2 processes considered in this paper, burning of fossil-fuel causes the highest O_2 flux. Additionally, the high fossil-fuel flux is mainly concentrated in regions where a high density of livestock and humans are located. The following regions are areas where the highest O_2 flux occurs: East Asia, India, North America, Europe, and central Africa. Normally, these areas should all be relatively developed areas with dense populations and intense human activities. However, situations are different in central Africa, an underdeveloped

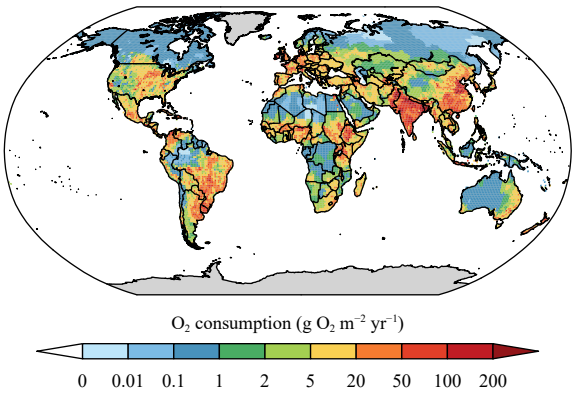

Fig. 5. The global distribution of O_2 fluxes due to livestock respiration in 2018.

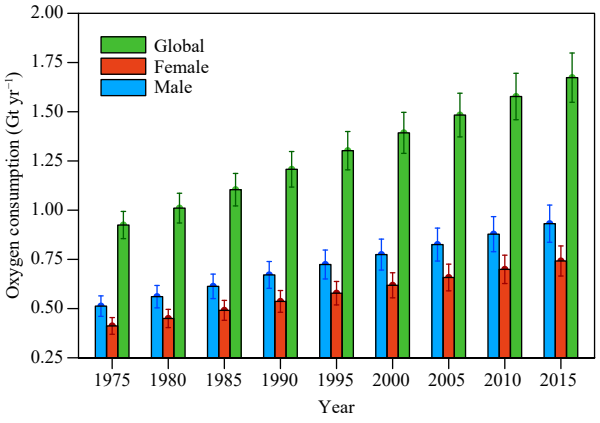

Fig. 6. The global total O_2 flux due to human respiration from 1975 to 2015 (Gt O_2 yr^{-1}). Blue, red, and green bars denote the consumption by males and females, and global total consumption. Standard deviations are also shown.

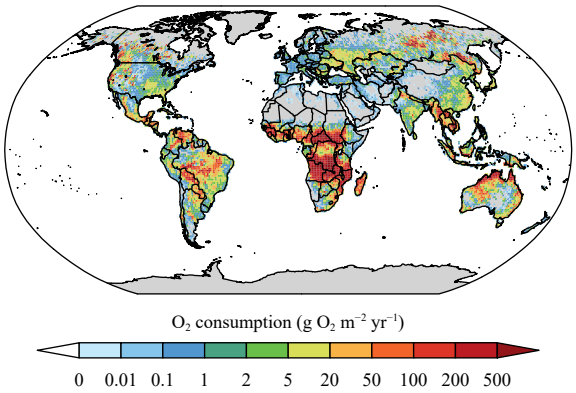

Fig. 7. The global pattern of O_2 fluxes due to wildfires in 2018.

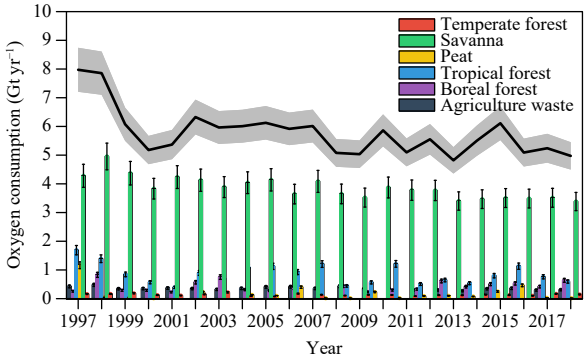

Fig. 8. The long-term trend in total O_2 consumption by each type of wildfires from 1997 to 2018, with standard deviations illustrated.

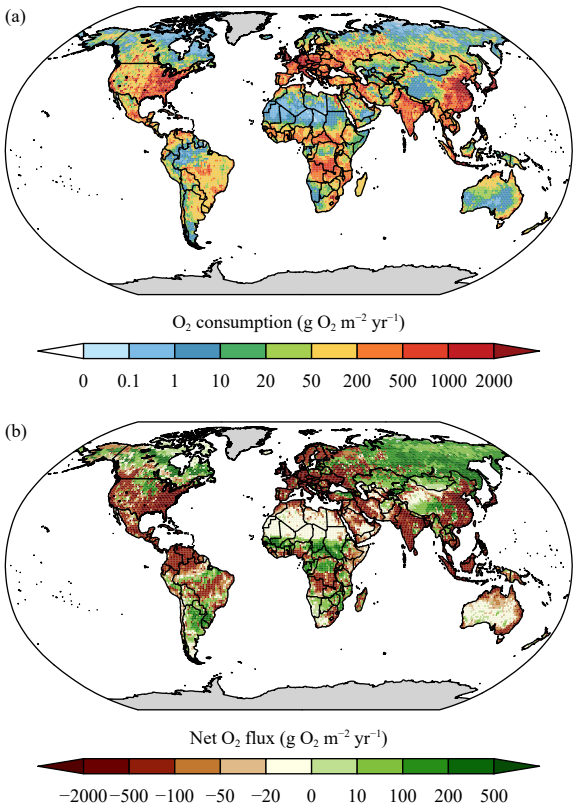

Fig. 9. Net terrestrial O_2 fluxes in the period of 2000–2018. (a) The averaged O_2 consumption and (b) net O_2 fluxes.

region where wildfires make the biggest contribution to local O_2 fluxes, which also displays a high level of the O_2 flux. The areas that cover Australia, the Tibetan Plateau, the Sahara Desert, and the Amazon rainforest are identified as the low O_2 consumption areas.

Estimation of the net biological O_2 flux over land is based on the result of Net Ecosystem Exchange (NEE) provided by the NOAA CarbonTracker, version CT2017 (from 2000 to 2016) and CT-NRT.v2019-2 (from 2017 to 2018; Peters et al., 2007). The O_2 flux caused by fire activities, which has been considered in the previous section in this paper, are excluded from NEE estimates. Areas with the negative flux (covered by brown colors, O_2 sink) denotes places where the land is consuming O_2 in the atmosphere, while areas with the positive flux (covered by green colors, O_2 source) indicate places where O_2 is produced. The global pattern of averaged net terrestrial O_2 flux averaged from 2000 to 2018, namely the result of NEE flux minus human-related flux, is shown in Fig. 9b. Since the positive O_2 flux from land is much smaller in magnitude than the negative flux, a modification of the color bar has been carried out so that the visualization is enhanced. Brown regions (East Asia, Europe, North America, and northern South America) indicate that human activities consume more O_2 than the local ecosystem's supply ability. The brown regions have occupied more than 50% of the global land surface. Green regions, including the Tibetan Plateau, northern Canada, and Siberia, represent regions that are still able to release O_2 to the atmosphere in spite of the local anthropogenic forcing.

At present, because of the worldwide intensification of energy consumption, population growth, overgrazing, etc., the human-related O_2 flux has been far greater than the terrestrial ecosystem's supply ability. Thus, the O_2 balance has already been disturbed, resulting in a steady decrease in the atmospheric O_2 concentration in the past decades. According to our estimation, it is revealed that during the period of 2000–2018, the O_2 consumption has experienced an increase from 33.69 ± 1.11 Gt O_2 yr^{-1} in 2000 to 47.63 ± 0.80 Gt O_2 yr^{-1} in 2018, whereas the land production (11.34 ± 13.48 Gt O_2 yr^{-1} averaged during the period from 2000 to 2018) has only increased slightly (Fig. 10).

With regards to the O_2 flux between the atmosphere and ocean, a hypothesis has already been widely accepted that the ocean might play a role as the O_2 source (positive flux) in the O_2 cycle. The climate change characterized by global warming has cut down the solubility of surface seawater (Bopp et al., 2002; Plattner et al., 2002), which directly results in a declining dissolved O_2 in the upper ocean. Thus, O_2 reserved in the ocean is gradually being released to the atmosphere. The exchange of O_2 between the air and sea is thought to be superimposed on the air–sea O_2 flux in the natural background of different timescales. It has been estimated that during the period of 2000–2010 the amount of O_2 outgassed from oceans was 1.4 Gt O_2 yr^{-1} (Keeling and Manning, 2014). Compared with the magnitude of other processes in the budget we proposed, this value is small enough to be ignored. In addition, the sparse coverage of observations over the ocean makes it challenging to provide a spatial distribution of air–sea O_2 with acceptable accuracy and reliability (Keeling et al., 2010).

3.5 *Uncertainty analysis and data validation*

Monte Carlo simulations were carried out to estimate uncertainties in the O_2 consumption for each component we calculated (see Section 2.2). The standard deviation in the total O_2 consumption flux in 2018 is 0.67 Gt O_2 yr^{-1}. Standard deviations (absolute uncertainty) and coefficients of variation (relative uncertainty) of the spatial distribution are shown in Fig. 11. Regions with a large standard deviation (greater than 200 g O_2 m^{-2} yr^{-1}) are consistent with those with high O_2 consumption (East Asia, India, Europe, and North America). Regions with a

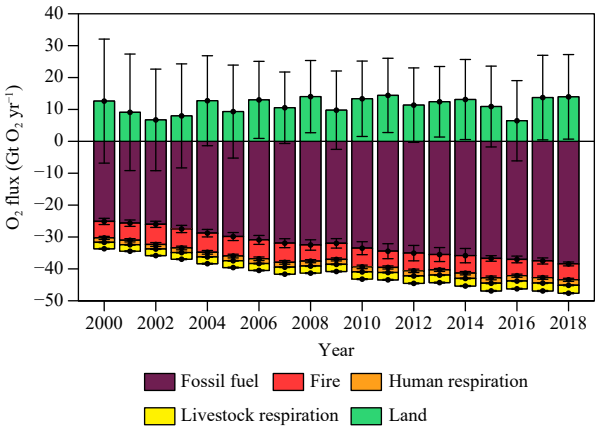

Fig. 10. The O_2 flux of each component in the budget from 2000 to 2018, with the standard deviation of each component illustrated.

small standard deviation (less than 10 g O_2 m^{-2} yr^{-1}) are consistent with those with low O_2 consumption (north of the Sahara Desert and Tibetan Plateau).

However, in terms of the relative uncertainty, large coefficients of variation (greater than 100%) are mainly found in regions with low O_2 flux (high-latitude areas in the Northern Hemisphere, north of the Sahara Desert, central Asia, and Southeast Asia). In areas with high O_2 consumption flux (East Asia, India, Europe, and North America), the coefficient of variation is mostly less than 30%. Our estimates exhibit better credibility in regions with high O_2 flux, implying that the main contributors are well captured in our estimates. More work is needed to reduce uncertainties in the regions with low O_2 consumption flux.

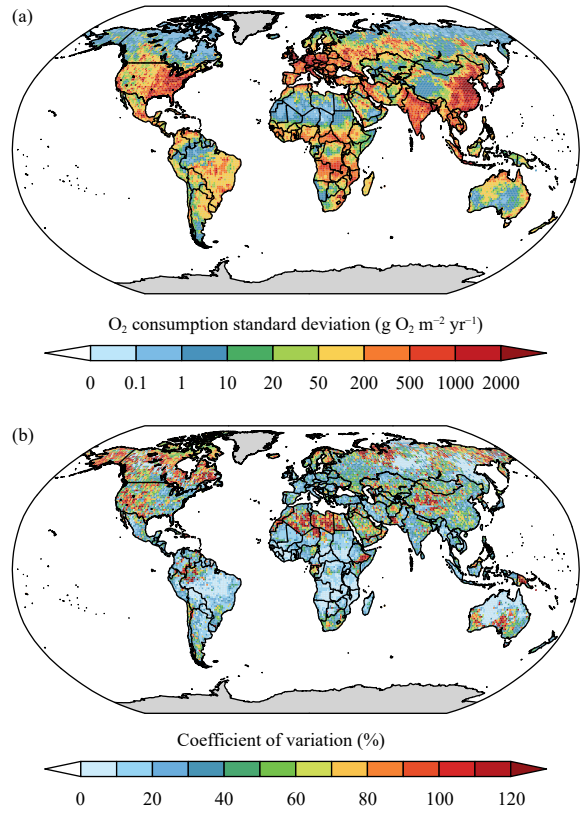

Fig. 11. Global distributions of absolute and relative uncertainties of the O_2 consumption. (a) Absolute uncertainties are shown as standard deviations and (b) relative uncertainties are shown as coefficients of variation (standard deviations/average values), where standard deviations and average values are obtained from each grid point calculated with 1000 Monte Carlo simulations.

For validation, we compared the observed annual changes in atmospheric O_2 with the estimated annual changes based on O_2 consumption fluxes at the global scale from 1997 to 2018. The estimated annual change (ΔO_2, Gt O_2 yr^{-1}) is calculated according to the following equation:

$$\Delta O_2 = -C_{\text{anthro}} + P_{\text{land}} + O_{\text{ocean}}, \quad (7)$$

where C_{anthro} (Gt O_2 yr^{-1}) is the O_2 consumption due to anthropogenic activities (excluding wildfires); P_{land} (Gt O_2 yr^{-1}) and O_{ocean} (Gt O_2 yr^{-1}) denote the net O_2 production from the land by photosynthesis and outgassing from the ocean, respectively. P_{land} and O_{ocean} are estimated based on the method used by Ishidoya et al. (2012), Tohjima et al. (2008), and Bender et al. (2005). The results indicate an average production of 10.14 Gt O_2 yr^{-1} from the land and outgassing of 0.89 Gt O_2 yr^{-1} from the ocean during the period 1997–2018. Figure 12a shows a comparison of the observed annual changes in O_2 (Keeling, 2019) and estimated annual changes. The observed global annual changes were calculated by using weighting functions according to the latitude of each station. The results have a correlation coefficient of 0.82 at the 99% confidence level and a regression coefficient of 1.16 with an intercept of −5.17 ± 9.85.

Figure 12b shows the difference between the estimated and observed annual changes in O_2 (estimated minus observed) during 1997–2018. The observed declines are faster than estimated changes before 2004, and slower after 2004. This may be explained by an underestimation of anthropogenic fluxes or overestimation of the O_2 production from land and ocean before 2004. Changes in the land production may be correlated with internal climate variabilities, such as the El Niño–Southern Oscillation (ENSO) and Pacific Decadal Oscillation (PDO). Further studies are required to elucidate impacts of the climate variability and human activities on the response of global O_2 cycles at both regional and global scales.

4. Future projections

In future scenarios, human activities will still play an

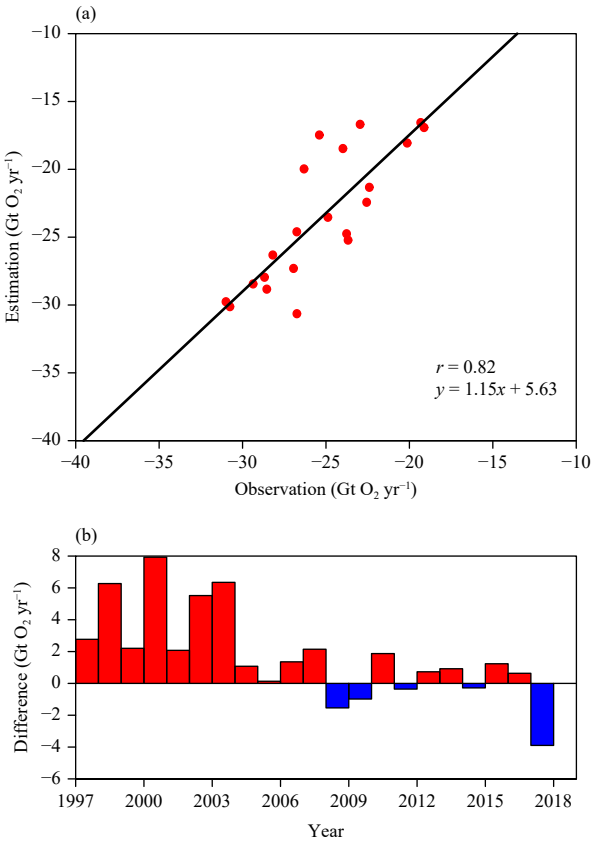

Fig. 12. (a) The comparison and (b) difference between the observed and estimated annual changes in O_2 from 1997 to 2018. The observed global annual change in O_2 is calculated with a weighting function based on the latitude of each station.

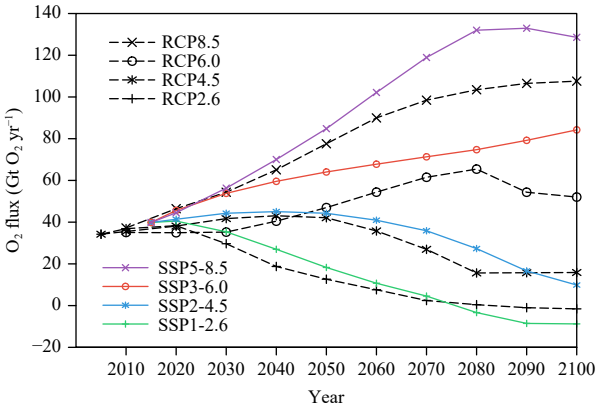

Fig. 13. Global O_2 fluxes in SSP and RCP scenarios in the 21st century. Positive and negative fluxes denote the removal of O_2 from atmosphere and the O_2 emission, respectively.

important role in modulating the global O_2 cycle. Here, we made an initial attempt to project the O_2 consumption in future scenarios based on the emission trajectories of CO_2 throughout the end of the 21st century. Four of the shared socioeconomic pathways (SSPs) used in the Coupled Model Intercomparison Project Phase 6 (CMIP6; Gidden et al., 2019) and four of the representative concentration pathways (RCPs) are selected in our estimations. From Fig. 13, we can see a significant increase in the O_2 consumption in RCP8.5 and SSP5-8.5, with the O_2 consumption higher than 100 Gt at the end of the 21st century. While in RCP2.6 and SSP1-2.6, negative fluxes will occur in the mid-2070s due to the popularization of biofuels. Biofuels can be carbon negative, which captures CO_2 from the atmosphere higher than that released during its production and combustion. Therefore, during the carbon sequestration via photosynthesis, O_2 is released into the atmosphere. It is, however, to be noted that OR is assumed to be independent of time (a constant value of 1.4, the current global average) in the estimation. In future scenarios, fuel types may vary when renewable energy is introduced and even becomes a dominant energy type. Here, we only present a rough estimation, which deserves further investigations in the future.

5. Conclusions and discussion

In this paper, a global dataset of the O_2 consumption on the grid scale is developed and compared with the biological O_2 flux to reveal the geographical location of the source and sink of atmospheric O_2. To our knowledge, this dataset is the first global map of O_2 consumption. The uncertainty is estimated based on the Monte Carlo method. The estimated dataset is also compared with observations for validation. The result indicates an increase in the O_2 consumption flux from 33.69 ± 1.11 Gt O_2 yr^{-1} in 2000 to 47.63 ± 0.80 Gt O_2 yr^{-1} in 2018. The combustion of fossil fuel and industrial activities (38.45 ± 0.61 Gt O_2 yr^{-1}) contribute the most, followed by wildfires (4.9 ± 0.48 Gt O_2 yr^{-1}) and respiration processes by livestock and humans (2.48 ± 0.16 and 1.73 ± 0.13 Gt O_2 yr^{-1}, respectively). The US, Europe, India, and East Asia are identified as the high O_2 consumption regions (with O_2 fluxes greater than 500 g O_2 m^{-2} yr^{-1}), while Australia, the Tibetan Plateau, the Sahara Desert, and the Amazon rainforest are identified as the low O_2 consumption areas. The O_2 sink regions (East Asia, Europe, North America, and northern South America) occupy more than 50% of the global land surface, while the O_2 source regions are mainly distributed in the Tibetan Plateau, northern Canada, and Siberia.

This dataset can be further improved by compiling other fuel-consumption data from different data sources. We also need to consider other potential impacts, including the climate and diet, on calculations of human and

livestock respiration. The updated data with a higher temporal resolution, including seasonal, weekly, and daily cycles for different fuel types, are also needed, so that monthly observations can be used for further validation.

Acknowledgments. We thank Julia Steinbach from Stockholm University and Christoph Gerbig from Max Planck Institute for Biogeochemistry for providing the CO_2 release and oxygen uptake from fossil fuel emission estimate (COFFEE) dataset. We thank Shixue Li from Hokkaido University for his valuable suggestions on this work.

REFERENCES

Andres, R. J., T. A. Boden, and G. Marland, 2016: Annual fossil-fuel CO_2 emissions: Mass of emissions gridded by one degree latitude by one degree longitude. ORNL/CDIAC-97, NDP-058, Carbon Dioxide Information Analysis Center, Oak Ridge National Laboratory, U.S. Department of Energy, Oak Ridge, Tenn, 56 pp, doi: 10.3334/CDIAC/ffe.ndp058.2016.

Battle, M., M. Bender, T. Sowers, et al., 1996: Atmospheric gas concentrations over the past century measured in air from firn at the South Pole. *Nature*, **383**, 231–235, doi: 10.1038/383231a0.

Bender, M. L., T. Sowers, J. M. Barnola, et al, 1994a: Changes in the O_2/N_2 ratio of the atmosphere during recent decades reflected in the composition of air in the firn at Vostok Station, Antarctica. *Geophys. Res. Lett.*, **21**, 189–192, doi: 10.1029/93GL03548.

Bender, M. L., T. Sowers, and L. Labeyrie, 1994b: The Dole Effect and its variations during the last 130,000 years as measured in the Vostok Ice Core. *Global Biogeochem. Cycles*, **8**, 363–376, doi: 10.1029/94GB00724.

Bender, M. L., D. T. Ho, M. B. Hendricks, et al., 2005: Atmospheric O_2/N_2 changes, 1993–2002: Implications for the partitioning of fossil fuel CO_2 sequestration. *Global Biogeochem. Cycles*, **19**, GB4017, doi: 10.1029/2004GB002410.

Bopp, L., C. Le Quéré, M. Heimann, et al., 2002: Climate-induced oceanic oxygen fluxes: Implications for the contemporary carbon budget. *Global Biogeochem. Cycles*, **16**, 6–1, doi: 10.1029/2001GB001445.

Cai, Q. X., X. D. Yan, Y. F. Li, et al., 2018: Global patterns of human and livestock respiration. *Sci. Rep.*, **8**, 9278, doi: 10.1038/s41598-018-27631-7.

Chen, S. Y., J. P. Huang, Y. Qian, et al., 2017: An overview of mineral dust modeling over East Asia. *J. Meteor. Res.*, **31**, 633–653, doi: 10.1007/s13351-017-6142-2.

Dintenfass, L., D. G. Julian, and G. V. F. Seaman, 1983: *Heart Perfusion, Energetics, and Ischemia*. Springer, Boston, MA, 663 pp, doi: 10.1007/978-1-4757-0393-1.

Frape, D., 2004: Equine Nutrition and Feeding (Third Edition). Blackwell Pub, Oxford, UK, 192–194.

Gidden, M. J., K. Riahi, S. J. Smith, et al., 2019: Global emissions pathways under different socioeconomic scenarios for use in CMIP6: A dataset of harmonized emissions trajectories through the end of the century. *Geosci. Model Dev.*, **12**, 1443–1475, doi: 10.5194/gmd-12-1443-2019.

Gilbert, M., G. Nicolas, G. Cinardi, et al., 2018: Global distribution data for cattle, buffaloes, horses, sheep, goats, pigs, chickens and ducks in 2010. *Sci. Data*, **5**, 180227, doi: 10.1038/sdata.2018.227.

Henry, C. J. K., 2005: Basal metabolic rate studies in humans: Measurement and development of new equations. *Public Health Nutr.*, **8**, 1133–1152, doi: 10.1079/PHN2005801.

Huang, J. G., Y. Bergeron, B. Denneler, et al., 2007: Response of forest trees to increased atmospheric CO_2. *Crit. Rev. Plant Sci.*, **26**, 265–283, doi: 10.1080/07352680701626978.

Huang, J. P., J. P. Huang, X. Y. Liu, et al., 2018: The global oxygen budget and its future projection. *Sci. Bull.*, **36**, 1180–1186, doi: 10.1016/j.scib.2018.07.023.

IPCC, 2006: *2006 IPCC Guidelines for National Greenhouse Gas Inventories*, Chapter 3, National Greenhouse Gas Inventory Programme, Institute for Global Environmental Strategies, Hayama, Japan, 10–106.

IPCC, 2014: *Climate Change 2013: The Physical Science Basis. Contribution of Working Group I to the Fifth Assessment Report of the Intergovernmental Panel on Climate Change*. Cambridge University Press, New York. 121–140.

Ishidoya, S., S. Aoki, D. Goto, et al., 2012: Time and space variations of the O_2/N_2 ratio in the troposphere over Japan and estimation of the global CO_2 budget for the period 2000–2010. *Tellus B.*, **64**, 18964, doi: 10.3402/tellusb.v64i0.18964.

Janssens-Maenhout, G., M. Crippa, D. Guizzardi, et al., 2019: EDGAR v4.3.2 global atlas of the three major greenhouse gas emissions for the period 1970–2012. *Earth Syst. Sci. Data*, **11**, 959–1002, doi: 10.5194/essd-11-959-2019.

Jones, H., 2003: Design Rules for Space Life Support Systems. SAE Technical Paper 2003-01-2356, doi: 10.4271/2003-01-2356.

Keeling, R. F., 1988: Development of an interferometric oxygen analyzer for precise measurement of the atmospheric O_2 mole fraction. PhD dissertation, Harvard University, Cambridge, 57–59.

Keeling, R. F., 2019: Atmospheric Oxygen Data for Alert, Cold Bay, Cape Kumukahi, La Jolla Pier, Mauna Loa Observatory, American Samoa, Cape Grim, Palmer Station and South Pole. [Available online at http://scrippso2.ucsd.edu/osub2sub-data].

Keeling, R. F., and A. C. Manning, 2014: Studies of recent changes in atmospheric O_2 content. *Treatise on Geochemistry*. 2nd ed, H. D. Holland, and K. K. Turekian, Eds., Elsevier Ltd., Amsterdam, 385–405, doi: 10.1016/B978-0-08-095975-7.00420-4.

Keeling, R. F., A. Körtzinger, and N. Gruber, 2010: Ocean deoxygenation in a warming world. *Annu. Rev. Mar. Sci.*, **2**, 199–229, doi: 10.1146/annurev.marine.010908.163855.

Kleiber, M., 1932: Body size and metabolism. *Hilgardia*, **6**, 315–353, doi: 10.3733/hilg.v06n11p315.

Le Quéré, C., R. M. Andrew, P. Friedlingstein, et al., 2018: Global carbon budget 2018. *Earth Syst. Sci. Data*, **10**, 2141–2194, doi: 10.5194/essd-10-2141-2018.

Li, Y. C., Y. F. Xu, M. Chu, et al., 2012: Influences of climate change on the uptake and storage of anthropogenic CO_2 in the global ocean. *J. Meteor. Res.*, **26**, 304–317, doi: 10.1007/s13351-012-0304-z.

Liu, X. Y., J. P. Huang, J. P. Huang, et al., 2019: Anthropogenic

oxygen flux from 1975 to 2012, link to NetCDF files. PANGAEA, doi: 10.1594/PANGAEA.899167.

Liu, Z., D. B. Guan, W. Wei, et al., 2015: Reduced carbon emission estimates from fossil fuel combustion and cement production in China. *Nature*, **524**, 335–338, doi: 10.1038/nature14677.

Luyssaert, S., I. Inglima, M. Jung, et al., 2007: CO_2 balance of boreal, temperate, and tropical forests derived from a global database. *Global Change Biol.*, **13**, 2509–2537, doi: 10.1111/j.1365-2486.2007.01439.x.

Martin, D., H. McKenna, and V. Livina, 2017: The human physiological impact of global deoxygenation. *J. Physiol. Sci.*, **67**, 97–106, doi: 10.1007/s12576-016-0501-0.

Murakami, D., and Y. Yamagata., 2019: Estimation of gridded population and GDP scenarios with spatially explicit statistical downscaling. *Sustainability*, **11**, 2106, doi: 10.3390/su11072106.

Peters, W., A. R. Jacobson, C. Sweeney, et al., 2007: An atmospheric perspective on North American carbon dioxide exchange: CarbonTracker. *Proc. Natl. Acad. Sci. USA*, **104**, 18,925–18,930, doi: 10.1073/pnas.0708986104.

Petsch, S. T., 2014: The global oxygen cycle. *Treatise on Geochemistry*. 2nd ed, H. D. Holland, and K. K. Turekian, Eds., Elsevier Ltd., Amsterdam, 437–473, doi: 10.1016/B978-0-08-095975-7.00811-1.

Plattner, G. K., F. Joos, and T. F. Stocker, 2002: Revision of the global carbon budget due to changing air–sea oxygen fluxes. *Global Biogeochem. Cycles*, **16**, 1096, doi: 10.1029/2001gb001746.

Royer, D. L., 2014: Atmospheric CO_2 and O_2 during the phanerozoic: Tools, patterns, and impacts. *Treatise on Geochemistry*. 2nd ed, H. D. Holland, and K. K. Turekian, Eds., Elsevier Ltd., Amsterdam, 251–267, doi: 10.1016/B978-0-08-095975-7.01311-5.

Shi, P. J., Y. Q. Chen, A. Y. Zhang, et al., 2019: Factors contribution to oxygen concentration in Qinghai–Tibetan Plateau. *Chinese Sci. Bull.*, **64**, 715–724, doi: 10.1360/n972018-00655.

Steinbach, J., C. Gerbig, C. Rödenbeck, et al., 2011: The CO_2 release and oxygen uptake from fossil fuel emission estimate (COFFEE) dataset: Effects from varying oxidative ratios. *Atmos. Chem. Phys.*, **11**, 6855–6770, doi: 10.5194/acp-11-6855-2011.

Stolper, D. A., M. L. Bender, G. B. Dreyfus, et al., 2016: A Pleistocene ice core record of atmospheric O_2 concentrations. *Science*, **353**, 1427–1430, doi: 10.1126/science.aaf5445.

Tilman, D., J. Hill, and C. Lehman, 2006: Carbon-negative biofuels from low-input high-diversity grassland biomass. *Science*, **314**, 1598–1600, doi: 10.1126/science.1133306.

Tohjima, Y., H. Mukai, Y. Nojiri, et al., 2008: Atmospheric O_2/N2 measurements at two Japanese sites: Estimation of global oceanic and land biotic carbon sinks and analysis of the variations in atmospheric potential oxygen (APO). *Tellus B.*, **60**, 213–225, doi: 10.1111/j.1600-0889.2007.00334.x.

United Nations, Department of Economic and Social Affairs, Population Division, 2019: *World Population Prospects 2019*. Department of Economic and Social Affairs Population Division, New York, 374 pp.

Valentino, F. L., M. Leuenberger, C. Uglietti, et al., 2008: Measurements and trend analysis of O_2, CO_2 and δ^{13} C of CO_2 from the high altitude research station Junfgraujoch, Switzerland—A comparison with the observations from the remote site Puy de Dôme, France. *Sci. Total Environ.*, **391**, 203–210, doi: 10.1016/j.scitotenv.2007.10.009.

van der Werf, G. R., J. T. Randerson, L. Giglio, et al., 2017: Global fire emissions estimates during 1997–2016. *Earth Syst. Sci. Data*, **9**, 697–720, doi: 10.5194/essd-9-697-2017.

Walpole, S. C., D. Prieto-Merino, P. Edwards, et al., 2012: The weight of nations: An estimation of adult human biomass. *BMC Public Health*, **12**, 439, doi: 10.1186/1471-2458-12-439.

Wang, R., S. Tao, P. Ciais, et al., 2013: High-resolution mapping of combustion processes and implications for CO_2 emissions. *Atmos. Chem. Phys.*, **13**, 5189–5203, doi: 10.5194/acp-13-5189-2013.

Zhai, P. M., B. Q. Zhou, and Y. Chen, 2018: A review of climate change attribution studies. *J. Meteor. Res.*, **32**, 671–692, doi: 10.1007/s13351-018-8041-6.

Tech & Copy Editor: Meili ZHANG